別紙３

学会発表　（2002～2004）

国内

学会記録（国内）

2002年

1.　武田元博、高山昌理子、小林正樹、中島護雄、楊明、大貫幸二、石田孝宣、大内憲明。乳腺腫瘍の生物フォトン画像計測１ー腫瘍の生物フォトン画像と組織像の相関．第61回日本癌学会総会、2002年10月1-3日、東京

2.　武田元博、大内憲明。極微弱生物フォトン計測技術の医療応用。第１回東北大学医工学シンポジウム、青葉記念会館、仙台、2002年7月12日

3.　大内憲明。東北大学における産学連携プログラム。第２回産学連携フォーラム-医学2002-知識と企業活力の出会い、東京、2002年12月18日。

2003年

1.　大内憲明。未来医療を拓く医工連携。日本学術会議・医用生体工学専門委員会ＭＥフォーラム2003

2.　大内憲明。ナノテクノロジーの医学・医療応用への期待。第2回メディカルインフォマテクスシンポジウム、東大駒場先端科学技術研究センター、東京、2003年3月27日。

3.　大内憲明。医療応用を目指したナノテクノロジー研究戦略。ナノ学会第１回大会、神戸、2003年5月29-31日。（特別講演）

4.　武田元博、中島護雄、石田孝宣、大貫幸二、大内憲明。新規計測用チャンバーを用いた乳腺腫瘍組織の生物フォトン画像計測。第103回日本外科学会総会、札幌、2003年6月4-6日。

5.　　武田元博、高山真理子、小林正樹、中島護雄、大貫幸二、石田孝宣、大内憲明。乳腺腫瘍の生物フォトン計測２-腫瘍組織と生物フォトン発光強度の相関。第62回日本癌学会、名古屋、2003年9月25-27日。

6.　中島護雄、武田元博、大内憲明、多田寛、小林正樹、鈴木聡、川添良幸、粕谷厚生。ナノサイズ蛍光ビーズを用いたセンチネルリンパ節診断法の検討。第62回日本癌学会、名古屋、2003年9月25-27日。

7.　多田寛、佐竹正延、亀井尚、武田元博、中島護雄、小林正樹、鈴木聡、川添良幸、粕谷厚生、大内憲明。ナノクリスタルを用いた乳癌細胞のイメージング。第62回日本癌学会、名古屋、2003年9月25-27日。

2004年

1. 大内憲明、ナノテクノロジーの医学・医療への応用-ナノメディシンへの期待第３回国際バイオＥＸＰＯ、東京ビッグサイト、2004年5月19-21日

2. 武田元博、中島護雄、石田孝宣、大貫幸二、大内憲明。新規ナノヨー化銀を用いたセンチネルリンパ節生検。第104回日本外科学会総会、大阪、2004年6月7-9日

3. 中島護雄、武田元博、石田孝宣、大貫幸二、大内憲明。蛍光ビーズを用いたセンチネルリンパ節生検法の検討。第104回日本外科学会総会、大阪、2004年6月7-9日。

4. 武田元博、小林芳男、三澤清登、中島護雄、多田寛、亀井尚、川添良幸、粕谷厚生、佐竹正延、大内憲明。AgIナノビーズを用いた新規Ｘ線造影剤の基礎的検討。第63回日本癌学会総会、福岡、2004年9月29日ー10月1日

5. 多田寛、佐竹正延、亀井尚、武田元博、中島護雄、樋口秀男、粕谷厚生、小林正樹、川添良幸、大内憲明。CdSeナノクリスタルを用いたHER2発現乳癌細胞の蛍光イメージング。第63回日本癌学会総会、福岡、2004年9月29日ー10月1日

6. 中島護雄、武田元博、多田寛、小林正樹、鈴木聡、小林芳男、三澤清登、川添良幸、粕谷厚生、大内憲明。ナノサイズシリカコーティング蛍光ビーズを用いたセンチネルリンパ節診断法の検討。第63回日本癌学会総会、福岡、2004年9月29日ー10月1日

7. 多田寛、佐竹正延、亀井尚、武田元博、中島護雄、川添良幸、粕谷厚生、大内憲明。CdSeナノクリスタルを用いたHER2発現乳癌細胞の蛍光イメージング。ナノ学会第２回大会、東京、2004年5月9-11日

8. 多田寛、佐竹正延、亀井尚、武田元博、中島護雄、川添良幸、粕谷厚生、大内憲明。CdSeナノクリスタルを用いたHER2発現乳癌細胞の蛍光イメージング。ナノ学会第２回大会、東京、2004年5月9-11日

9. 石井聡、大野かおる、Kumar V、川添良幸。金属原子内包シリコンクラスターのGW計算。ナノ学会第２回大会、東京、2004年5月9-11日

10. 本郷研太、前園涼、Kumar V、川添良幸、安原洋。量子モンテカルロ法によるCr@Si12クラスターの研究。ナノ学会第２回大会、東京、2004年5月9-11日

11. 斐英造、長内弘喜、Kumar V、川添良幸。ロジウムクラスターの非調蜜構造と磁性。ナノ学会第２回大会、東京、2004年5月9-11日

12. 伊藤正寛、Kumar V、川添良幸。第一原理計算。ナノ学会第２回大会、東京、2004年5月9-11日

13. 高木直、樋口秀男。生細胞内におけるCdSeナノクリスタルの１粒子検出。ナノ学会第２回大会、東京、2004年5月9-11日

14. 佐藤崇、樋口秀男。蛍光性CdSe粒子によるモータータンパク質の高精度位置解析。ナノ学会第２回大会、東京、2004年5月9-11日

15. 亀井敬、角田世治、樋口秀男。単一生体ナノモーターの協同的な高次運動機能。ナノ学会第２回大会、東京、2004年5月9-11日

16. 樋口秀男、亀井敬、佐藤崇、渡辺朋信。ナノ粒子を標識したモータータンパク質の動きのnm, ms分解能計測。ナノ学会第２回大会、東京、2004年5月9-11日

国際（海外）

Ohuchi N. Japan (NCI-JSPS) Cooperative Cancer Research Program Scientist Exchange Summary Report.
The United States-Japan Cooperative Cancer Research Program Annual Report: April 2000 through March 2001.
The National Cancer Institute and Japan society for the Promotion of Scinece. 2002

Ohuchi N, et al. Performance parameter evaluation of mammography screening in women aged 40-49: a comparison with women aged 50-69.

The Biennial Meeting of the International Breast Cancer Screening Network, Montpellier, France, May 30-31, 2002.

Ohuchi N. Recent sdvances in the diagnosis and treatment of breast cancer.
The 14th Annual Meeting of the Chinese General surgery, Changsha, China, June 15-19, 2002.

Ohuchi N. Current Review of Breast Cancer Diagnosis and treatment in Japan.
The China-Japan Medical Conference at The Jurin University, Chanchung, China, August 25-29, 2002.

Ohuchi N. Innovative Achievements in Cancer Imaging - Mammography for Screening and MRI for Breast-conserving Surgery.

The 33rd International Symposium of the Princess Takamatsu Cancer Research Fund, Tokyo, November 11-14, 2002.

Ohuchi N, Takeda M, Kawazoe Y, Kasuya A, Kamei T, Satake M. Biophoton Cancer Imaging and Generation of Nano-size Sensing Capsule.

The 1st Symposium on Future Medical Engineering Based on Bio-nanotechnology, Sendai, January 28, 2003.

Ohuchi N, Kawazoe Y, Kasuya A, Takeda M, Nakajima M, Tada H, Kamei T, Satake M. Nano-Size Sensing Capsule for Future Medical Application,
The 1st Nanomedicine Workshop, Honolulu, USA, March 19, 2003.

Takeda M, **Ohuchi1 N**, Nakajima M, Tada H, Kobayashi M. Innovative Cancer Imaging by Biophoton Emission.
The 1st Nanomedicine Workshop, Honolulu, USA, March 19, 2003.

Tada H, Kamei T, Satake M, Takeda M, Nakajima M, Kasuya A, Kawazoe Y, **Ohuchi N**. Breast cancer cell imaging by nanocrystals semiconductor quantum dots conjugated with anti-HER2 antibody. 24th Congress of the International Association for Breast Cancer Research, Sacramento, CA, USA, November 1-5, 2003

Suzuki A, Shiraishi K, **Ohuchi N**, Sato T, Das I, Kitajewski J. Generation of Transgenic Mouse to Conditionally Active Notch1 Signaling. 24th Congress of the International Association for Breast Cancer Research, Sacramento, CA, USA, November 1-5, 2003

Higuchi H, Watanabe T, Tada H, **Ohuchi N**. Frontier of nano-biology and nano-medicine. The 5th Internal symposium on Future Medical Engineering based on Bio-nanotechnology, Nano-science and Technology for Medical Application. Sendai, February 2005.

Kasuya A, Takeda M, Nakajima M, Kamei T, **Ohuchi N**, Kobayashi Y, Kobayashi M. Application of nanoparticles for optical fluorescence probe and X-ray CT in biomedicine. The 5th Internal symposium on Future Medical Engineering based on Bio-nanotechnology, Nano-science and Technology for Medical Application. Sendai, February 2005.

Nakajima M, Takeda M, Kobayashi M, Suzuki S, **Ohuchi N**. Nano-sized fluorescent particles as new tracers for sentinel node detection: an experimental model for determination of appropriate size and wavelength.The 5th Internal symposium on Future Medical Engineering based on Bio-nanotechnology, Nano-science and Technology for Medical Application. Sendai, February 2005.

Tada H, Higuchi H, Watanabe T, Kamei T, **Ohuchi N**. In vivo breast cancer cell imaging with semiconductor quantum dots conjugated with monoclonal anti-Her 2 antibody. The 5th Internal symposium on Future Medical Engineering based on Bio-nanotechnology, Nano-science and Technology for Medical Application. Sendai, February 2005.

Li S, Nakazato M, Yoshida n, Ogata T, Kon s, tolfer J, Rothenberg E, Watanabe T, Satake M, **Ohuchi N**. An effort to investigate the functional difference of transcription factor Renx1 isoforms derived from two distinct promoters. The 5th Internal symposium on Future Medical Engineering based on Bio-nanotechnology, Nano-science and Technology for Medical Application. Sendai, February 2005.

Takeda M, Kobayashi M, Nakajima M, Kasuya A, **Ohuchi N**. Biophoton imaging for detection of cancer growth. The 5th Internal symposium on Future Medical Engineering based on Bio-nanotechnology, Nano-science and Technology for Medical Application. Sendai, February 2005.

Ohuchi N, Tada H, Higuchi H, Kasuya A. Generation of CdSe nanocrystal semiconductor quantum dots conjugated with anti-HER2 antibody for molecular imaging of breast cancer. The AACR Special Conference 2005: Oncogenomics, San Diego, CA, 2005

別紙４

特許財産権の出願登録状況　(2002～2003年)

内容	発明者	権利者	知的財産権の種	番号	出願年月日	取得年月日
多重粒子及びその製造方法	川添良幸 粕谷厚生	川添良幸 粕谷厚生 佐竹正延 大内憲明 東レ・ダウコーニング株	特許	2004-210549	2002/12/26	2002/12/26
センチネルリンパ節検出剤及びその検出方法	武田元博 大内憲明	武田元博 大内憲明 川添良幸 粕谷厚生 佐竹正延 東レ・ダウコーニング株	特許	2004-269439	2003/3/10	2003/3/10
Ｘ線造影剤及び造影方法	武田元博 小林芳男	大内憲明 川添良幸 粕谷厚生 佐竹正延 東レ・ダウコーニング株	特許	特願2005-042634	2005/2/18	

Ⅳ. 研究成果の刊行物・別刷

ELSEVIER

Colloids and Surfaces A: Physicochem. Eng. Aspects 251 (2004) 197–201

COLLOIDS AND SURFACES A

www.elsevier.com/locate/colsurfa

Silica-coating of AgI semiconductor nanoparticles

Yoshio Kobayashi[a], Kiyoto Misawa[a], Motohiro Takeda[b], Masaki Kobayashi[c], Masanobu Satake[d], Yoshiyuki Kawazoe[e], Noriaki Ohuchi[b], Atsuo Kasuya[f], Mikio Konno[a,*]

[a] *Department of Chemical Engineering, Graduate School of Engineering, Tohoku University, 07 Aoba, Aramaki-aza, Aoba-ku, Sendai 980-8579, Japan*
[b] *Division of Surgical Oncology, Graduate School of Medicine, Tohoku University, Seiryo-machi, Aoba-ku, Sendai 980-8574, Japan*
[c] *Department of Electronics, Tohoku Institute of Technology, Kasumi-cho, Taihaku-ku, Sendai 982-8577, Japan*
[d] *Institute of Development, Aging and Cancer, Tohoku University, Seiryou-machi, Aoba-ku, Sendai 980-8575, Japan*
[e] *Institute for Materials Research, Tohoku University, Katahira, Aoba-ku, Sendai 980-8577, Japan*
[f] *Center for Interdisciplinary Research, Tohoku University, Aoba, Aramaki-aza, Aoba-ku, Sendai 980-8578, Japan*

Received 29 July 2004; accepted 7 October 2004

Abstract

A method for silica-coating of AgI nanoparticles is proposed, which applies Stöber method in the presence of a silane coupling agent, 3-mercaptopropyltrimethoxysilane (MPS), with the use of dimethylamine (DMA) catalyst for alkoxide hydrolysis. The AgI nanoparticles were prepared from $AgClO_4$ and KI. The silica-coating was performed with 0–2.3×10^{-5} M MPS, 11–20 M water, 0–0.1 M DMA and 0.0004–0.15 M tetraethyl orthosilicate (TEOS). The addition of MPS suppressed generation of free silica particles and improved uniformity of shell thickness. Silica shells were formed at water concentrations of 11–15 M, but excess water (20 M) caused aggregation of free silica particles, and resulted in formation of gel network. The silica shell thickness could be varied from 3 to 33.0 nm as the TEOS concentration was increased from 0.0004 to 0.04 M at 4.5×10^{-6} M MPS under the condition of 11 M water and 0.01 M DMA.

Keywords: AgI; Nanoparticle; Core-shell; Silica coating; Sol–gel; Stöber method

1. Introduction

Nano-sized semiconductor particles such as CdS, CdSe and AgI attract special interest because they are in an intermediate state between atoms or molecules and bulk material, and can be expected to exhibit excellent properties different from bulk material [1–3].

A common technique for stabilizing nanoparticles is the use of surface active agents or macromolecular substances that are adsorbed to particle surface to form a physical barrier against other approaching particles. The coating of the particles with inert silica shells can also be used as a stabilizing technique [4–9]. Role of the silica shell is two-fold, since it not only provides a greatly enhanced colloidal stability in water, but also can be used to control distance between core particles within assemblies through shell thickness.

From this view point, extensive studies on silica-coated nanoparticles have been made [5,7]. The method of the silica-coating was composed of three steps: (1) modification of the nanoparticle surface to make it vitreophilic by using silane coupling agents with an amino or thiol group such as 3-aminopropyltrimethoxysilnae and 3-mercaptopropyltrimethoxysilane (MPS), (2) slow silica deposition in water from a sodium silicate solution, and (3) extensive growth of the silica shells through sol–gel reaction of silicon alkoxide in ethanol/ammonia mixtures [5]. The silica deposition in the sodium silicate solution requires long-time if silica shells are to be grown to certain thickness. In addition, the sodium silicate possibly introduces impurities to the particles. Therefore, a simplified and more rapid method with no sodium silicate is desirable.

* Corresponding author. Tel.: +81 22 217 7239; fax: +81 22 217 7241.
E-mail address: konno@mickey.che.tohoku.ac.jp (M. Konno).

0927-7757/$ – see front matter © 2004 Elsevier B.V. All rights reserved.
doi:10.1016/j.colsurfa.2004.10.007

A study on preparing silica-coated AgI nanoparticles was performed by Giersig et al. [10]. They showed that silica-coated Ag nanoparticles that were prepared according to the ref. [7] were mixed with I_2 solution, in which I_2 molecules diffused in silica shell layer, and eventually transforming the Ag nanoparticles inside to AgI nanoparticles. However, long-time processes with sodium silicate were required, and generation of AgI nanoparticles also took place on external silica surface. We have recently developed [11,12] a technique for direct silica-coating of metal nanoparticles in one single step without need of sodium silicate, which is based on Stöber method. In the present work, the direct silica-coating method was extended to silica-coating of AgI nanoparticles in the presence of MPS.

2. Experimental

2.1. Chemicals

Silver perchlorate ($AgClO_4$) (Kanto Chemical Co. Inc., 99%) and potassium iodide (KI) (Wako Pure Chemicals Ltd., 99.5%) were used as silver precursors. Tetraethyl orthosilicate (TEOS) (Wako Pure Chemicals Ltd., 95%), MPS (Aldrich, 97%) and ethanol (Wako Pure Chemicals Ltd., 99.5%) were used for silica-coating, and DMA (Wako Pure Chemicals Ltd., 50%) was used as catalysts for a sol–gel reaction of TEOS and MPS. All chemicals were used as received. Ultrapure deionized water (resistivity higher than 18 MΩ cm) was used in all the preparations.

2.2. Preparation of materials

2.2.1. AgI nanoparticles

Colloids of AgI nanoparticles were prepared by mixing of $AgClO_4$ and KI. Freshly prepared 0.015 ml of 0.2 M $AgClO_4$ in H_2O was added to 6 ml of 0.001 M KI under vigorous stirring at room temperature. Color of the mixture turned yellow immediately. Fig. 1 gives absorption spectrum of AgI nanoparticle colloid. A sharp peak around 421 nm and a shoulder peak around 330 nm were attributed to exciton peaks of AgI [13–16], which provided an evidence for generation of AgI particles. Typically, spherical AgI nanoparticles with an average size of 23.8 nm were observed in TEM (see inset of Fig. 1).

2.2.2. Silica-coating

Stöber method with TEOS was applied to silica-coating of the AgI nanoparticles. Six millilitres of the AgI colloid was added to 0.1 ml of 0.00135 M MPS in H_2O. After 15 min, 24 ml of ethanol and successively 0.0266 ml of TEOS were added to the colloid. Then, the silica-coating was initiated by rapidly injecting an aqueous DMA solution into the AgI/TEOS colloid. The concentrations of TEOS and water were ranged from 0.0004 to 0.15 M and from 11 to 20 M, respectively.

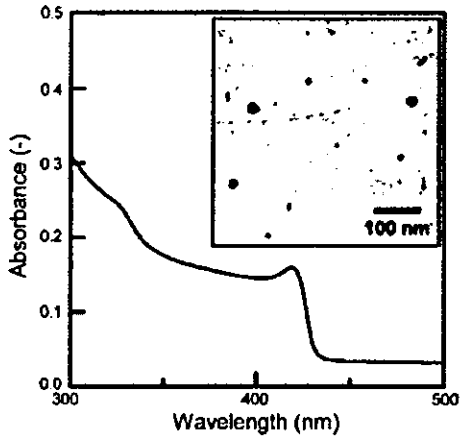

Fig. 1. TEM image and UV–vis absorption spectrum of AgI colloid in ethanol/water.

2.3. Characterization

The silica-coated AgI ($AgI–SiO_2$) nanoparticles were characterized by transmission electron microscopy (TEM) and ultraviolet (UV)–visible (vis) spectroscopy. TEM was performed with a Zeiss LEO 912 OMEGA microscope operating at 100 kV. Samples for TEM were prepared by dropping and evaporating the nanoparticle suspensions on a collodion-coated copper grid. Silica shell thickness was estimated as the difference between silver particle and composite particle sizes. UV–vis extinction spectra were measured with a Hitachi UV-3010 spectrophotometer.

3. Results and discussion

3.1. Effect of MPS concentration

Fig. 2 shows TEM micrographs of $AgI–SiO_2$ nanoparticles prepared at various MPS concentrations. In Fig. 2a and b, many core-free silica particles and shell-free AgI nanoparticles were observed, though a few core-shell particles were present. Probably, silica did not have a strong affinity for the AgI nanoparticle surfaces during growth from silica nuclei to silica nanoparticle. Particles in Fig. 2c and d had core-shell structures composed of the AgI core with a size of 13.5 nm and the silica shell with a thickness of 15.1 nm. MPS molecules possibly had strong affinity for AgI surface so that condensation reaction between MPS and TEOS was initiated on the surface.

3.2. Effect of water concentration

Fig. 3 shows TEM micrographs of $AgI–SiO_2$ nanoparticles prepared at water concentrations from 11 to 20 M. All the DMA concentrations were 0.01 M in a series of the experiments. The water concentration of 11 M was the lower limit in the present experimental, because the water

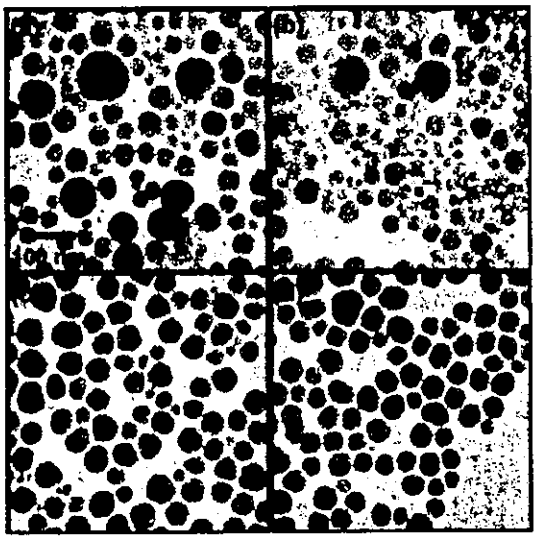

Fig. 2. TEM images of AgI–SiO_2 prepared at MPS concentrations of 0 (a), 4.5×10^{-7} (b), 4.5×10^{-6} (c) and 2.3×10^{-5} M (d). Initial concentrations of water, DMA and TEOS were 11, 0.01 and 0.004 M, respectively.

concentration in the commercial DMA solution is 50% and adjusting the DMA concentration to 0.01 M provided the water concentration of 11 M at lowest. AgI–SiO_2 core-shell particles were observed in Fig. 3a and b. The AgI cores that were observed in Fig. 3b were large, compared to Fig. 3a. As the water concentration rises, DMA is dissociated and consequently ionic strength increases in turn [17]. Since the increase in ionic strength reduces electrostatic repulsion between the AgI nanoparticles, the reduction of electrostatic repulsion probably promoted the aggregation and growth of AgI nanoparticles. It was also observed in Fig. 3b that many core-free silica particles with a size of 22.1 nm were

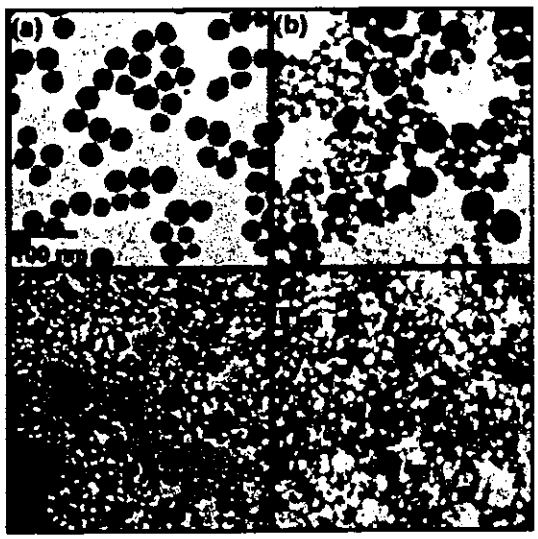

Fig. 3. TEM images of AgI–SiO_2 prepared at water concentrations of 11 (a), 12 (b), 15 (c) and 20 M (d). Initial concentrations of MPS, DMA and TEOS were 4.5×10^{-6}, 0.01 and 0.004 M, respectively.

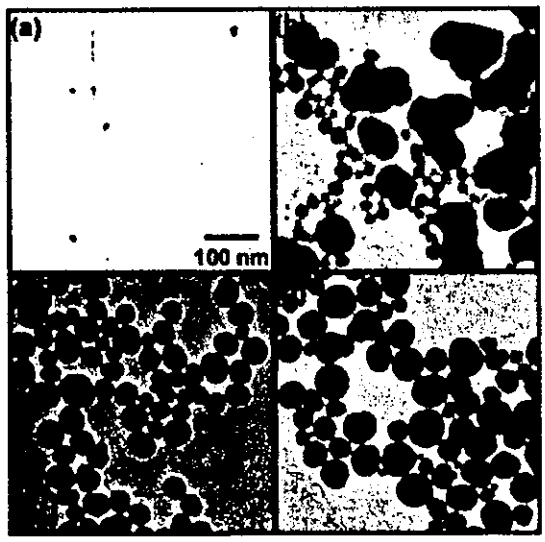

Fig. 4. TEM images of AgI–SiO_2 prepared at DMA concentrations of 0 (a), 0.005 (b), 0.01(c) and 0.1 M (d). Initial concentrations of MPS, water and TEOS were 4.5×10^{-6}, 11 and 0.004 M, respectively.

generated. The increase in ionic strength due to the dissociation of DMA reduces electrostatic repulsion not only between AgI nanoparticles but also between silica nuclei generated with hydrolysis of TEOS. Consequently, the silica nuclei aggregated and grew as the silica nanoparticles with the increase in water concentration. In Fig. 3c, network structures were formed, though some AgI–SiO_2 core-shell particles were still observed. In Fig. 3d, no core-shell particles were formed. Further increase in ionic strength at high water concentration probably promoted aggregation of silica nanoparticles and succeeding formation of gel network structures.

3.3. *Effect of DMA concentration*

Fig. 4 shows TEM micrographs of AgI–SiO_2 nanoparticles prepared at different DMA concentrations. At a DMA concentration of 0 M (Fig. 4a), no silica shell and no silica particle was observed because of a shortage of the catalyst. At 0.005 M (Fig. 4b), particles that contained multiple cores and core-free silica particles were obtained. At 0.01 M, core-free silica particles were obtained a little and the AgI nanoparticles were coated with silica with a thickness of 15.1 nm (Fig. 4c). An increase in the concentration to 0.1 M increased silica shell thickness to 16.6 nm (Fig. 4d). Addition of DMA is considered to increase the ionic strength of the solution due to the dissociation and catalyzes the hydrolysis and condensation of the alkoxysilanes [18]. Thus, the high DMA concentration should reduce the double layer repulsion between the AgI nanoparticles and the silica nuclei. As a result, the silica nuclei were deposited on the AgI particle surfaces and then the silica shells grew.

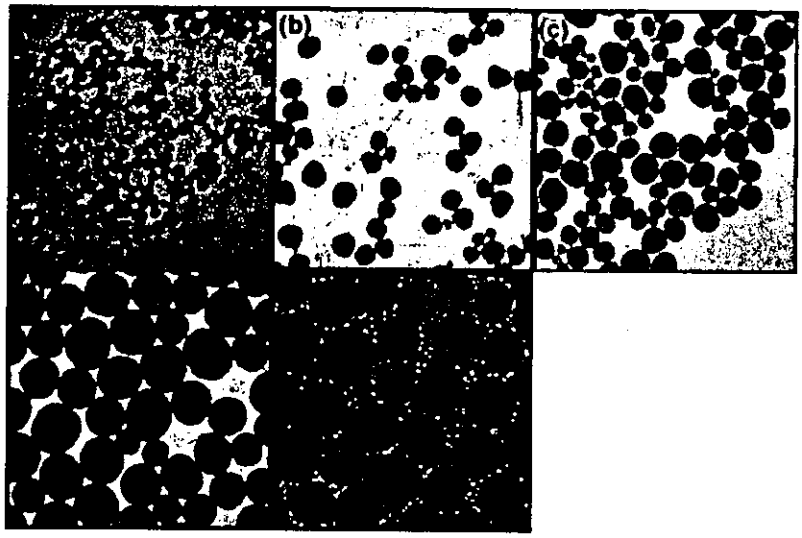

Fig. 5. TEM images of AgI–SiO_2 prepared at TEOS concentrations of 0.0004 (a), 0.002 (b), 0.004 (c), 0.04 (d) and 0.15 M (e). Initial concentrations of MPS, DMA and water were 4.5×10^{-6}, 0.01 and 11 M, respectively.

3.4. Effect of TEOS concentration

For the control of shell thickness, TEOS concentration was varied in the experiments of Fig. 5 a–e. At [TEOS] = 0.0004–0.04 M (Fig. 5a–d), most of the particles were quasi-perfect core-shells with just one AgI core and the shell thickness increased from 3.0 to 33.0 nm. Thus, the TEOS concentration was found to control the silica shell thickness within a certain threshold. However, further addition of TEOS ([TEOS] = 0.15 M) did not increase the shell thickness, and generated a large amount of core free silica particles, as shown in Fig. 5e.

3.5. UV–vis spectroscopy

Fig. 6 gives absorption spectra of AgI–SiO_2 colloid. In the spectra in Fig. 6a through c, a sharp peak around 421 nm and a shoulder peak around 330 nm were observed, which were the typical absorption spectra of the AgI nanoparticles. As the shell thickness increased, these peaks seemed to be screened by the strong scattering from the silica shell.

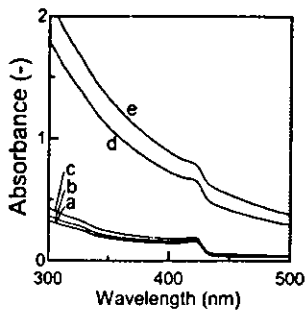

Fig. 6. UV–vis absorption spectra of AgI–SiO_2. Refer to Fig. 5 for symbols.

Although the shoulder peak was not clearly seen in Fig. 6d and e, the absorption peak of the AgI nanoparticles appeared around 421 nm in these figures. Thus, the existence of AgI nanoparticles was confirmed from the UV–vis spectroscopy.

4. Conclusion

A synthetic method for AgI–SiO_2 core-shell particles was developed. The method was based on the deposition of a silica shell on the AgI cores. The silica-coating was performed with a sol–gel reaction of TEOS in the presence of the AgI nanoparticles. At high water concentrations, no formation of homogeneous silica shells could be performed. With increasing TEOS concentration, the silica shell thickness increased. Concentration effects can probably be explained by the difference in ionic strength of the solution.

Acknowledgements

This research was partially supported by the Ministry of Education, Culture, Sports, Science and Technology of Japan (Grant-in-Aid for the COE project, Giant Molecules and Complex Systems), and by the Ministry of Health, Labor and Welfare of Japan.

References

[1] L. Brus, J. Phys. Chem. 90 (1986) 2555.
[2] A.I. Ekimov, A.L. Efros, A.A. Onushchenko, Solid State Commun. 88 (1993) 947.
[3] K. Kimura, Z. Phys. D 11 (1989) 327.

[4] L.M. Liz-Marzán, M. Giersig, P. Mulvaney, Chem. Commun. (1996) 731.
[5] L.M. Liz-Marzán, M. Giersig, P. Mulvaney, Langmuir 12 (1996) 4329.
[6] M.A. Correa-Duarte, M. Giersig, L.M. Liz-Marzán, Chem. Phys. Lett. 286 (1998) 497.
[7] T. Ung, L.M. Liz-Marzán, P. Mulvaney, Langmuir 14 (1998) 3740.
[8] S.R. Hall, S.A. Davis, S. Mann, Langmuir 16 (2000) 1454.
[9] P. Mulvaney, L.M. Liz-Marzán, M. Giersig, T. Ung, J. Mater. Chem. 10 (2000) 1259.
[10] M. Giersing, T. Ung, L.M. Márzan, P. Mulvaney, Adv. Mater. 9 (1997) 570.
[11] E. Mine, A. Yamada, Y. Kobayashi, M. Konno, L.M. Liz-Marzán, J. Colloid Interface Sci. 264 (2003) 385.
[12] Y. Kobayashi, H. Katakami, E. Mine, D. Nagao, M. Konno, L. M. Liz-Marzán, J. Colloid Interface Sci., in press.
[13] H. Vogelsang, O. Husberg, W. Von der Osten, J. Lumin. 86 (2000) 87.
[14] S. Kondo, T. Itoh, T. Saito, Phys. Rev. B 57 (1998) 13235.
[15] P.S. Kumar, P.B. Dayal, C.S. Sunandana, Thin Solid Films 357 (1999) 111.
[16] Y. Wang, J. Mo, W. Cai, L. Yao, L. Zhang, Mater. Lett. 56 (2002) 502.
[17] G.H. Bogush, M.H. Tracy, C.F. Zukoski, J. Non-Crystal. Solids 104 (1988) 95.
[18] D. Nagao, Y. Kon, T. Satoh, M. Konno, J. Chem. Eng. Japan 33 (2000) 468.

ELSEVIER

Colloids and Surfaces A: Physicochem. Eng. Aspects 242 (2004) 47–52

COLLOIDS AND SURFACES A

www.elsevier.com/locate/colsurfa

Silica-coating of fluorescent polystyrene microspheres by a seeded polymerization technique and their photo-bleaching property

Yoshio Kobayashi [a,*], Kiyoto Misawa [a], Masaki Kobayashi [b], Motohiro Takeda [c], Mikio Konno [a], Masanobu Satake [d], Yoshiyuki Kawazoe [e], Noriaki Ohuchi [c], Atsuo Kasuya [f]

[a] *Department of Chemical Engineering, Graduate School of Engineering, Tohoku University, 07 Aoba, Aramaki-aza, Aoba-ku, Sendai 980-8579, Japan*
[b] *Department of Electronics, Tohoku Institute of Technology, Kasumi-cho, Taihaku-ku, Sendai 982-8577, Japan*
[c] *Division of Surgical Oncology, Graduate School of Medicine, Tohoku University, Seiryo-machi, Aoba-ku, Sendai 980-8574, Japan*
[d] *Institute of Development, Aging and Cancer, Tohoku University, Seiryou-machi, Aoba-ku, Sendai 980-8575, Japan*
[e] *Institute for Materials Research, Tohoku University, Katahira, Aoba-ku, Sendai 980-8577, Japan*
[f] *Center for Interdisciplinary Research, Tohoku University, Aoba, Aramaki-aza, Aoba-ku, Sendai 980-8578, Japan*

Received 30 October 2003; accepted 20 April 2004

Abstract

This paper describes silica-coating of polystyrene microspheres incorporated with fluorescence dyes (fluorescent microspheres) by means of a seeded polymerization technique based on Stöber method. The silica-coating of the fluorescent microspheres was performed in the presence of 0–10 g/l polyvinylpyrrolidone (PVP), 1.13–17 M water, 0–1.2 M aqueous ammonia and 0.00038–0.2 M tetraethoxyorthosilicate (TEOS). The addition of PVP was found to suppress the generation of free silica particles and improve the uniformity of shell thickness. The silica shell thickness increased from 13 to 138 nm with an increase in TEOS concentration at 10 g/l PVP, 0.4 M aqueous ammonia and 10.9 M water. The thickness also increased with the ammonia concentration and the water concentration. However, excess ammonia and water caused aggregation of free silica particles and the polystyrene microspheres. The silica-coated fluorescence microspheres showed more stable fluorescence to laser-irradiation than uncoated microspheres.

Keywords: Fluorescent microsphere; Core-shell; Silica-coating; Sol–gel; Seeded polymerization

1. Introduction

Microspheres incorporated with fluorescence dyes (fluorescent microspheres) have been used widely as cell-surface antigen detection, neutral retrograde tracers, phagocytosis tracers, sensitive diagnostic reagents and blood flow measurements [1–4]. It is desirable that fluorescences of dyes in the microspheres are strong and persistent for long periods. The photostability of the dyes is environmentally sensitive, and singlet state oxygen molecules play the main role of photo-bleaching of the fluorescence dye molecules in the excited state [5–7]. Core-shell type particles are good candidates for preventing decomposition because the shell materials can keep dyes from contact with oxygen molecules.

The core-shell types particles show various unique properties owing to their composite structures. They are applicable to a wide variety of materials such as magnetism [8–12], electronics [13–16] and optics [17–19]. Liz-Marzán and co-workers demonstrated silica-coating on CdS nanoparticles inhibited light-induced surface reactions, so that photostability of CdS was improved [20]. Our group also reported a protection effect of silica shell using silica-coated Co nanoparticles, in which the silica-coating prevented Co nanoparticles from oxidization and provided crystallization to cubic metal Co phase that showed magnetic properties [21]. In addition, we employed direct silica-coating on gold nanoparticles by a seeded polymerization techniques [22].

In this article, the silica-coating technique is extended to the fluorescence microspheres. The fluorescence microspheres have been coated with silica shell at different concentrations of polyvinylpyrrolidone (PVP), water, ammonia and tetraethoxysilane (TEOS). The photo-bleaching of the

* Corresponding author. Tel.: +81 22 217 7242; fax: +81 22 217 7293.
E-mail address: yoshio@mickey.che.tohoku.ac.jp (Y. Kobayashi).

0927-7757/$ – see front matter © 2004 Elsevier B.V. All rights reserved.
doi:10.1016/j.colsurfa.2004.04.052

fluorescence dyes within the microspheres has been monitored under irradiation of laser in the presence of air.

2. Experimental

2.1. Chemicals

FluoSpheres® beads (F-8803) commercially available from Molecular Probes Inc. were used as fluorescent microspheres. The fluorescent microspheres were composed of a host matrix of polystyrene and a dopant of fluorescent dyes. Fig. 1 shows their fluorescence spectrum and photograph taken by a transmission electron microscope (TEM). The fluorescent microspheres have a fluorescence peak at 512 nm and an average size of 193 nm. The chemicals of ethanol (99.5%), NH_4OH (25% aqueous solution) and tetraethylorthosilicate (TEOS, 95%) obtained from Wako Pure Chemicals Ltd., and polyvinylpyrrolidone (PVP, average molecular weight: 36000) from Nacalai Tesque Ltd. were used as received. Ultrapure deionized water (resistivity higher than 18 MΩ cm) was used in the preparations.

2.2. Preparation of materials

Silica-coating of the fluorescent microspheres was carried out with ammonia-catalyzed reaction of TEOS in ethanol–water solution in a hermetically sealed reactor equipped with a magnetic stirrer at room temperature. Ethanol solution of TEOS was added to aqueous PVP solution under vigorous stirring after addition of the suspension of the fluorescent microspheres. Hydrolysis reaction of TEOS was initiated by the addition of the aqueous ammonia solution to form silica shell on the microspheres, which

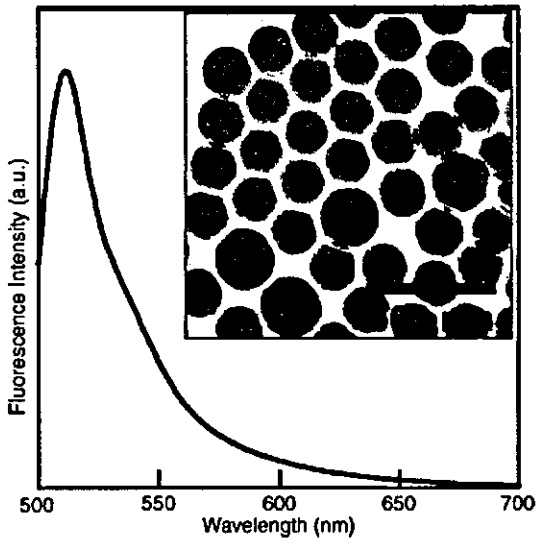

Fig. 1. Fluorescence spectrum of FluoSpheres® (F-8811) and their TEM image shown in the inset. The excitation wavelength was 488 nm.

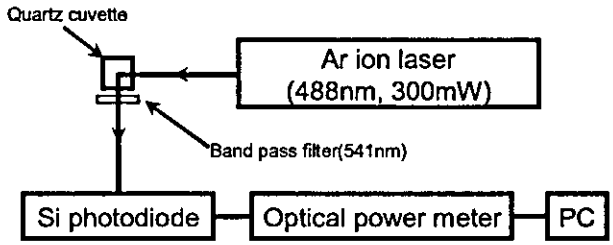

Fig. 2. Experimental set-up for measurements of photo-bleaching.

was reacted for 24 h under stirring. Concentrations of PVP, water, ammonia and TEOS and were in ranges of 0–10 g/l, 1.13–17 M, 0–1.2 M and 0.00038–0.2 M, respectively.

2.3. Characterization

The silica-coated fluorescent microspheres were observed with a transmission electron microscope (TEM) (Zeiss LEO 912 OMEGA) operated at 100 kV accelerating voltage. Samples for TEM were prepared by dropping the suspension of the fluorescent microspheres onto the top of a collodion-coated copper grid and drying. Fluorescence spectra were measured with a Hitachi F-4500 fluorophotometer. Fig. 2 shows a set-up for analysis of photo-bleaching. The silica-coated microspheres in a quartz cuvette were irradiated by an argon ion laser (Coherent, INOVA90) with an emission wavelength of 488 nm and a power of 300 mW. Fluorescence at 541 nm was selected using a band pass filter with a bandwidth of 10 nm and detected with an Si photodiode (Anritsu, MA9411A) connected with an Anritsu ML9001 optical power meter.

3. Results and discussion

3.1. Effect of PVP concentration

Fig. 3 shows TEM micrographs of silica-coated fluorescent microspheres prepared at various PVP concentrations. In whole images, many core-free silica particles with sizes of 50–80 nm were observed. According to Kawahashi and Shiho [23–25], PVP is required for preventing aggregation of particles. However, no aggregations of the fluorescent microspheres were observed even without the addition of PVP (Fig. 3(a)). The fluorescent microspheres used have carboxyl groups on their surfaces according to a commercial catalog of FluoSpheres® beads. These carboxyl groups probably prevent such aggregation. In Fig. 3(a) and (b), silica particles with sizes of 45–90 nm deposited on the surfaces of fluorescent microspheres, which indicated that silica did not have a strong affinity for the fluorescent microsphere surfaces during growth from silica nuclei to silica nanoparticle. Such deposition decreased with the increase in PVP concentration. In Fig. 3(c) (e), the silica shell with a size of 40–45 nm was formed on the surfaces, though the deposited

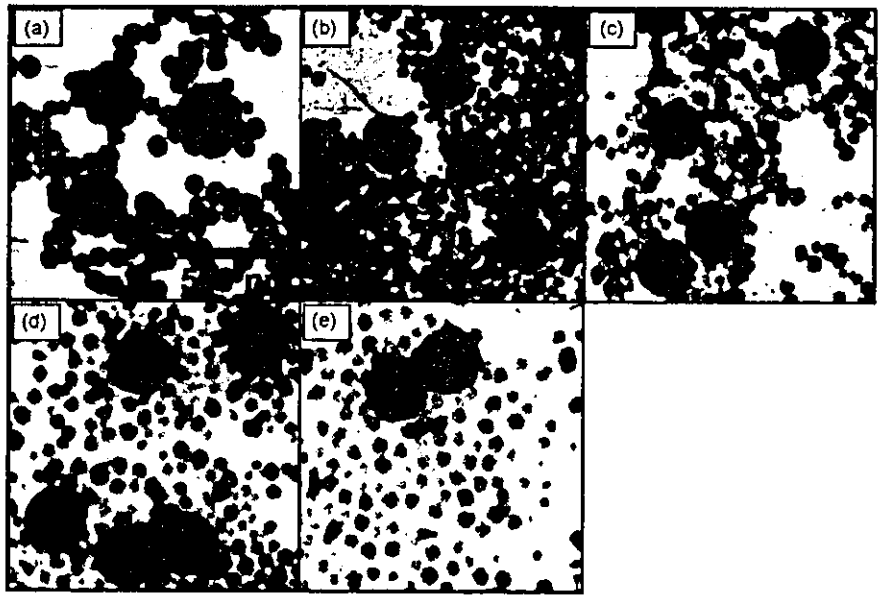

Fig. 3. TEM images of fluorescence microspheres coated with silica for 10.9 M water, 0.4 M ammonia and 0.02 M TEOS at PVP concentrations of (a) 0 g/l, (b) 0.01 g/l, (c) 0.1 g/l, (d) 1.0 g/l and (e) 10 g/l.

silica particles were still observed in Fig. 3(c). The surfaces of silica shell were smoother with the increase in PVP concentration. In our research, it can be considered that PVP improved an affinity between the silica nuclei and the fluorescent microsphere surfaces.

3.2. Effect of water concentration

Fig. 4 shows TEM micrographs of silica-coated fluorescent microspheres prepared at various water concentrations. In Fig. 4(a)–(c), homogeneous silica shells were observed on the surfaces of the fluorescent microspheres and their thickness increased from 13 to 60 nm with the water concentration. As Bogush and Zukoski reported [26], an increase in water concentration in TEOS/NH_3/water/ethanol solution dissociates ammonium hydroxide and brings about an increase in electric conductivity that corresponds to ionic strength. Since the increase in ionic strength reduces electrostatic repulsion between particles, the growth of silica shells was probably promoted.

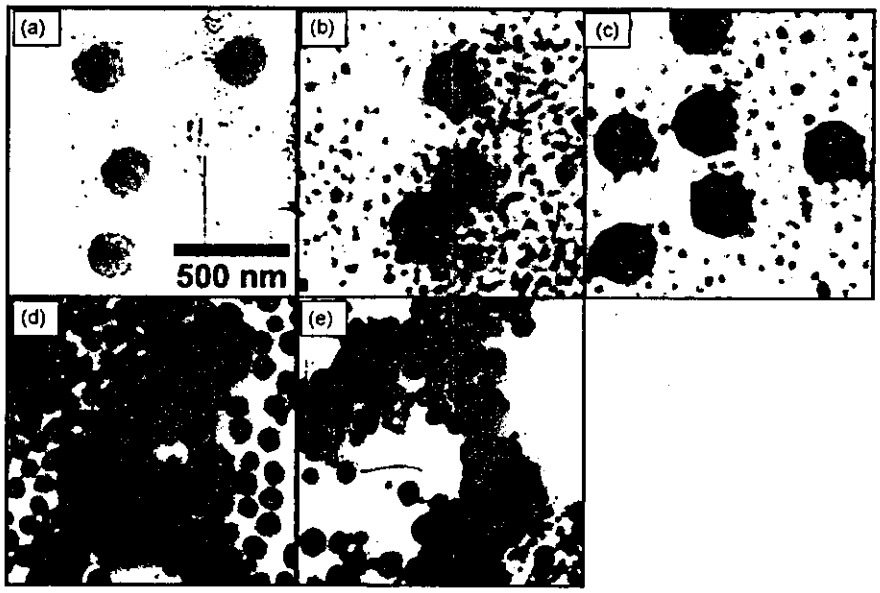

Fig. 4. TEM images of fluorescence microspheres coated with silica for 10 g/l PVP, 0.4 M ammonia and 0.02 M TEOS at initial water concentrations of (a) 1.13 M, (b) 5.0 M, (c) 10.9 M, (d) 13.0 M and (e) 17 M.

Many core-free silica particles were also observed and their average sizes increased from 41 to 92 nm with the water concentration. In Fig. 4(d) and (e), such silica particles adhered to the fluorescent microsphere surfaces and no more homogeneous shell was observed, which can not be explained by the change in ionic strength that was the factor causing the silica shell growth as shown in Fig. 4(a) (c). Because the dielectric constant of water/ethanol mixture increases with water concentration, silanol groups on the silica particle surface probably tend to ionize with increasing water concentration. This might increase affinity of the silica particles for the dispersant. Therefore, silica nuclei generated during the early stages of the sol–gel reaction probably grew as stable core-free silica particles.

3.3. Effect of ammonia concentration

Fig. 5 shows TEM micrographs of silica-coated fluorescent microspheres prepared at different ammonia concentrations. At an ammonia concentration of 0 M (Fig. 5(a)), no silica shell and no silica particle was observed because of a shortage of catalyst. At ammonia concentrations of 0.2–0.8 M (Fig. 5(b) (d)), the thickness of silica shell increased from 38 to 43 nm with the increase in ammonia concentration. Addition of ammonia increases the ionic strength of the solution and catalyzes the hydrolysis and condensation of the alkoxysilanes [27]. Thus, the high ammonia concentration should reduce the double layer repulsion between the fluorescent microspheres and the silica nuclei. As a result, the silica shells grew on the microsphere surfaces. At an ammonia concentration as high as 1.2 M, the fluorescent microspheres aggregated with the secondary generated silica particles (Fig. 5(e)). The high ammonia concentration extensively accelerated the sol–gel reaction of TEOS and then the core-free silica particles were generated from the silica nuclei and grew much before the silica nuclei was used for the silica shell formation.

3.4. Effect of TEOS concentration

Fig. 6 shows TEM micrographs of silica-coated fluorescent microspheres formed at various TEOS concentrations. Some silica particles were observed and their size tended to increase with the TEOS concentration. The ionic strength decreases as a sol–gel reaction of TEOS proceeds and then secondary silica particles are generated [28,29]. Since the high TEOS concentration should increase a source of silica, the silica shell grew. The silica shell thickness was varied from 13 to 138 nm as initial TEOS concentration increased from 0.00038 to 0.2 M. This means the shell thickness can be controlled within a certain threshold. The thickness of silica was smaller than those estimated from initial TEOS concentrations, because of the generation of the core-free silica particles.

3.5. Photo-bleaching

Fig. 7 shows the time-dependence of the fluorescence intensity. The fluorescence intensity of the silica-coated fluorescent microspheres was lower than that of the uncoated ones up to 15 min. However, the laser-irradiation over 15 min reversed the order of the fluorescence intensites. For making clear a difference between the silica-coated microspheres and the uncoated ones, the fluorescence intensities were normalized by the value of fluorescence intensity measured before the laser-irradiation, as shown in

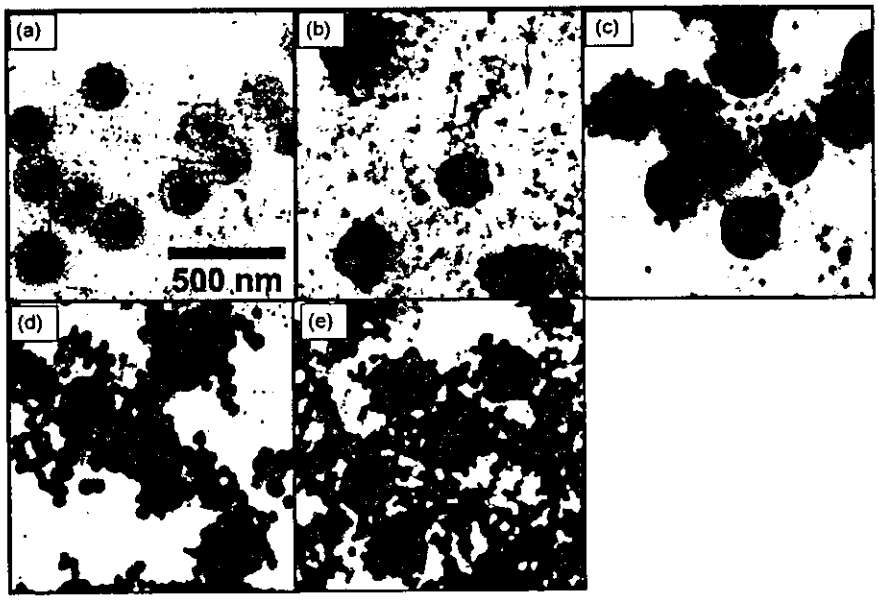

Fig. 5. TEM images of fluorescence microspheres coated with silica for 10 g/l PVP, 10.9 M water and 0.02 M TEOS at initial ammonia concentrations of (a) 0 M, (b) 0.2 M, (c) 0.4 M, (d) 0.8 M and (e) 1.2 M.

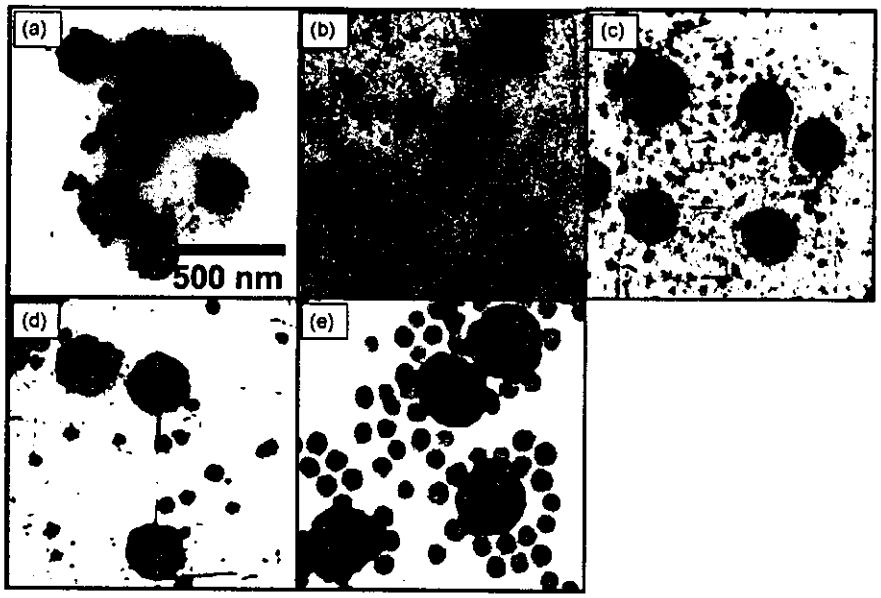

Fig. 6. TEM images of fluorescence microspheres coated with silica for 10 g/l PVP, 10.9 M water and 0.4 M ammonia at initial TEOS concentrations of (a) 0.00038 M, (b) 0.0015 M, (c) 0.009 M, (d) 0.02 M and (e) 0.2 M.

the inset. Time-dependence of the normalized fluorescence intensity for the silica-coated fluorescent microspheres was weak compared to that of the uncoated fluorescent microspheres, which is evidence that the silica-coated fluorescent microspheres were more stable in respect to their luminescence property than the uncoated ones. Singlet state oxygen molecules decompose dye molecules in their exited stage. [5–7]. This stable fluorescence property is probably related to the diffusional limitations of oxygen molecules inside of the fluorescent microspheres through the silica shell. Such stabilization by the silica-coating will be of importance in the preparation of stable materials for practical applications.

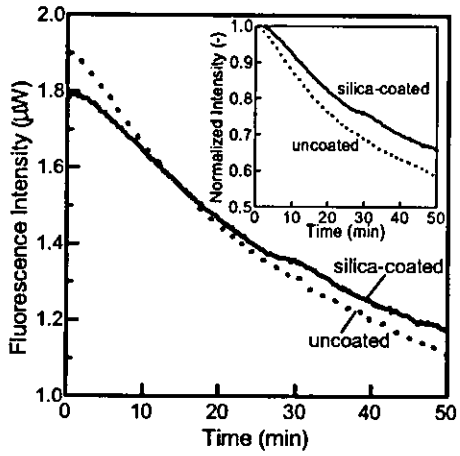

Fig. 7. Fluorescence intensities of silica-coated fluorescent microspheres and uncoated ones as a function of laser-irradiation time. The silica-coating was employed at 10 g/l PVP, 10.9 M water, 0.4 M ammonia and 0.02 M TEOS. The inset shows fluorescence intensity normalized by the value of fluorescence intensity measured before the laser-irradiation.

4. Conclusion

A synthetic method was developed for the stabilization of fluorescent microspheres. The method was based on the deposition of a silica shell on the fluorescent microsphere cores. The silica-coating was performed with a sol–gel reaction of TEOS in the presence of PVP and the fluorescent microspheres. Homogeneous silica shells were formed on the fluorescent microspheres in the presence of PVP. At high water and ammonia concentrations, no formation of homogeneous silica shells could be performed. With increasing TEOS concentration, the silica shell thickness increased. Concentration effects can probably be explained by differences in ionic strength of the solution. It was observed that the silica-coated fluorescent microspheres provided high luminescence stability, compared with uncoated ones. This property is significant for biomedical application.

Acknowledgements

This research was partially supported by the Ministry of Education, Culture, Sports, Science and Technology of Japan (Grant-in-Aid for the COE Project, Giant Molecules and Complex Systems), and by the Ministry of Health, Labor and Welfare of Japan.

References

[1] D.A.A. Vignali, J. Immunol. Methods 243 (2000) 243.
[2] M. Altun, E. Bergman, B. Ulfhake, J. Neurosci. Methods 108 (2001) 19.
[3] K.L. Kellar, M. Iannone, Exp. Hematol. 20 (2002) 1227.

[4] G. De Visscher, M. Haseldonckx, W. Flameng, M. Borgers, R.S. Reneman, K. van Rossem, J. Neurosci. Methods 122 (2003) 149.
[5] T. Suratwala, Z. Gardlund, K. Davidson, D.R. Uhlmann, S. Bonilla, N. Peyghambarian, J. Sol–Gel Sci. Technol. 8 (1997) 953.
[6] S. Singh, V.R. Kanetkar, G. Sridhar, V. Muthuswamy, K. Raja, J. Lumin. 101 (2003) 285.
[7] G. Qian, Y. Yang, Z. Wang, C. Yang, Z. Yang, M. Wang, Chem. Phys. Lett. 368 (2003) 555.
[8] F. Caruso, A.S. Susha, M. Giersig, H. Möhwald, Adv. Mater. 11 (1999) 950.
[9] F.G. Aliev, M.A. Correa-Duarte, A. Mamedov, J.W. Ostrander, M. Giersig, L.M. Liz-Marzán, N.A. Kotov, Adv. Mater. 11 (1999) 1006.
[10] J.-I. Park, J. Cheon, J. Am. Chem. Soc. 123 (2001) 5743.
[11] M. Wu, Y.D. Zhang, S. Hui, T.D. Xiao, S. Ge, W.A. Hines, J.I. Budnick, J. Appl. Phys. 92 (2002) 491.
[12] Y. Lu, Y. Yin, B.T. Mayers, Y. Xia, Nano Lett. 2 (2002) 183.
[13] S.M. Marinakos, D.A. Shultz, D.L. Feldheim, Adv. Mater. 11 (1999) 34.
[14] G. Oldfield, T. Ung, P. Mulvaney, Adv. Mater. 12 (2000) 1519.
[15] L.Y. Wang, Y.-J. Lin, W.-Y. Chiu, Synth. Met. 119 (2001) 155.
[16] H. Shiho, N. Kawahashi, Colloid Polym. Sci. 279 (2001) 1231.
[17] L.M. Liz-Marzán, M. Giersig, P. Mulvaney, Langmuir 12 (1996) 4329.
[18] M.A. Correa-Duarte, M. Giersig, L.M. Liz-Marzán, Chem. Phys. Lett. 286 (1998) 497.
[19] A. Rogach, A. Susha, F. Caruso, G. Sukhorukov, A. Kornowski, S. Kershaw, H. Möhwald, A. Eychmüller, H. Weller, Adv. Mater. 12 (2000) 333.
[20] M.A. Correa-Duarte, M. Giersig, L.M. Liz-Marzán, Chem. Phys. Lett. 286 (1998) 497.
[21] Y. Kobayashi, M. Horie, M. Konno, B. Rodríguez-González, L.M. Liz-Marzán, J. Phys. Chem. B 107 (2003) 7420.
[22] E. Mine, A. Yamada, Y. Kobayashi, M. Konno, L.M. Liz-Marzán, J. Colloid Interface Sci. 264 (2003) 365.
[23] H. Shiho, N. Kawahashi, J. Mater. Chem. 10 (2000) 2294.
[24] H. Shiho, N. Kawahashi, J. Colloid Interface Sci. 226 (2000) 91.
[25] H. Shiho, N. Kawahashi, Colloid Polym. Sci. 278 (2000) 270.
[26] G.H. Bogush, C.F. Zukoski, J. Colloid Interface Sci. 142 (1991) 1.
[27] E. Mine, M. Konno, J. Chem. Eng. Jpn. 34 (2001) 545.
[28] D. Nagao, Y. Kon, T. Satoh, M. Konno, J. Chem. Eng. Jpn. 33 (2000) 468.
[29] D. Nagao, T. Satoh, M. Konno, J. Colloid Interface Sci. 232 (2000) 102.

Biophoton detection as a novel technique for cancer imaging

Motohiro Takeda,[1] Masaki Kobayashi,[2] Mariko Takayama,[3] Satoshi Suzuki,[2] Takanori Ishida,[1] Kohji Ohnuki,[1] Takuya Moriya[4] and Noriaki Ohuchi[1,5]

[1]Division of Surgical Oncology, [3]Division of Dermatology and [4]Division of Pathology, Tohoku University Graduate School of Medicine, 1-1 Seiryo-machi, Aoba-ku, Sendai 980-8574; and [2]Division of Electronics, Tohoku Institute of Technology, 35 Kasumi-cho, Yagiyama, Taihaku-ku, Sendai 982-8577

(Received February 16, 2004/Revised June 16, 2004/Accepted June 16, 2004)

Biophoton emission is defined as extremely weak light that is radiated from any living system due to its metabolic activities, without excitation or enhancement. We measured biophoton images of tumors transplanted in mice with a highly sensitive and ultra-low noise CCD camera system. Cell lines employed for this study were AH109A, TE4 and TE9. Biophoton images of each tumor were measured 1 week after carcinoma cell transplantation to estimate the tumor size at week 1 and the biophoton intensity. Some were also measured at 2 and 3 weeks to compare the biophoton distribution with histological findings. We achieved sequential biophoton imaging during tumor growth for the first time. Comparison of microscopic findings and biophoton intensity suggested that the intensity of biophoton emission reflects the viability of the tumor tissue. The size at week 1 differed between cell lines, and the biophoton intensity of the tumor was correlated with the tumor size at week 1 (correlation coefficient 0.73). This non-invasive and simple technique has the potential to be used as an optical biopsy to detect tumor viability. (Cancer Sci 2004; 95: 656–661)

Ultraweak biophoton emission is defined as extremely weak light originating from living things as a result of their metabolic activities. This phenomenon has been recognized to occur without enhancement or excitement by chemical administration or light irradiation. Ultraweak biophoton emission ranges from the ultraviolet to the near infrared, and its intensity is generally lower than 10^{-9} W/cm^2, i.e., less than 1/1000 of the human visible light intensity.

Many living systems have been shown to exhibit biophoton emission since the invention of photo-multiplier tubes,[1] including proliferating *Saccharomyces cerevisiae*, longitudinal sections of bamboo shoot, injured soybean seedlings and fertilizing sea urchins.[2–5] All the results are consistent with pathological or physiological significance of biophoton emission. Samples from human beings, including smoker's breath and serum, also exhibit ultraweak light emission.[6] Thus, biophoton emission may be an indicator of pathological conditions in patients.

Cancer is a major cause of human mortality, and many diagnostic methods have been developed. Trials on ultraweak biophoton measurement of the serum or urine from cancer patients have also been performed for diagnostic applications.[7,8] Elevation of ultraweak light intensity from serum or urine has been attributed to metabolic changes in patients. Thus, measurement of carcinoma lesions might provide more accurate information on the pathological status of cancer. Shimizu *et al.* measured biophoton intensity from transplanted malignant tumors[9] and observed differences among the tumors, and Amano *et al.* presented biophoton images of bladder cancer transplanted in nude mice.[10] Although these results suggest the feasibility of biophoton measurement for cancer diagnosis, there has been no report discussing applications based on specific pathological features for cancer diagnosis.

In a recent study, we detected changes in biophoton emission from proliferating carcinoma cell cultures using a flow culture system coupled with a highly sensitive apparatus.[11] In the present study, TE9, an esophageal carcinoma cell line, exhibited quite similar changes in biophoton intensity during cell proliferation, and we measured the specific biophoton spectrum of a cell culture for the first time. The results demonstrated the applicability of biophoton measurement to the detection of cell proliferation for cancer diagnosis. Growth rate is one of the most important of the factors that define malignancy, and the results lead to the idea that biophoton emission may reflect the growth potential of the tumor.

In the present study, we investigated the relationship between biophoton intensity and tumor size after 1 week to ascertain the relationship of biophoton properties with the tumor growth potential. Furthermore, we took weekly measurements of the biophoton images of 3 different types of tumor for 2 or 3 weeks and compared them with the tumor histology to clarify the relationship between tissue distribution and the two-dimensional biophoton emission image. The feasibility of specific application of biophoton imaging is discussed.

Materials and Methods

Instrumentation. For the imaging of ultraweak light emission, a cooled charge-coupled device (CCD) camera system (ATC200C, Photometrics, Inc.) was utilized. A back-illuminated type of CCD (TK1024AB2, Tektronix, Inc.) is incorporated in the camera system with cooling at −120°C using liquid nitrogen. The camera head is mounted on a completely light-tight chamber, which includes a temperature-controlled mounting bed to maintain the body temperature of a mouse (Fig. 1).[12] A lens system (Nikor F/1.2, Nikon) was used for imaging an observation area measuring 100×100 mm. The CCD has a spectral sensitivity over the wavelength range from 400 to 1000 nm with a maximum quantum efficiency of 73% at 700 nm. Pixel size of the CCD is 24×24 μm with 1024×1024 format. In the experiments, the CCD camera was operated in 2×2 binning mode, with a resulting spatial resolution of 48×48 μm, which corresponded to a resolution of 190 μm on the object. Integration time for each measurement was 1 h. The minimum detectable intensity of the emission on a sample surface under the above condition is estimated to be 1.0×10^4 photons/s/cm^2, taking into account read-out noise and the dark current of the CCD, and the total light detection efficiency of the system. One count of the intensity indicated in figures corresponds to 1.64×10^4 photons emitted on the surface.

Image processing was made based on grey scale images of tumors. The images in figures shown in this article were further modified by converting emission intensity to specific colors according to a color bar (Fig. 2). Image processing for elimination of background noise induced by high-energy particles was applied with threshold filtering. The average emission intensity in the total region of the tumor was evaluated after subtraction of

[5]To whom correspondence should be addressed. E-mail: noriaki-o@umin.ac.jp

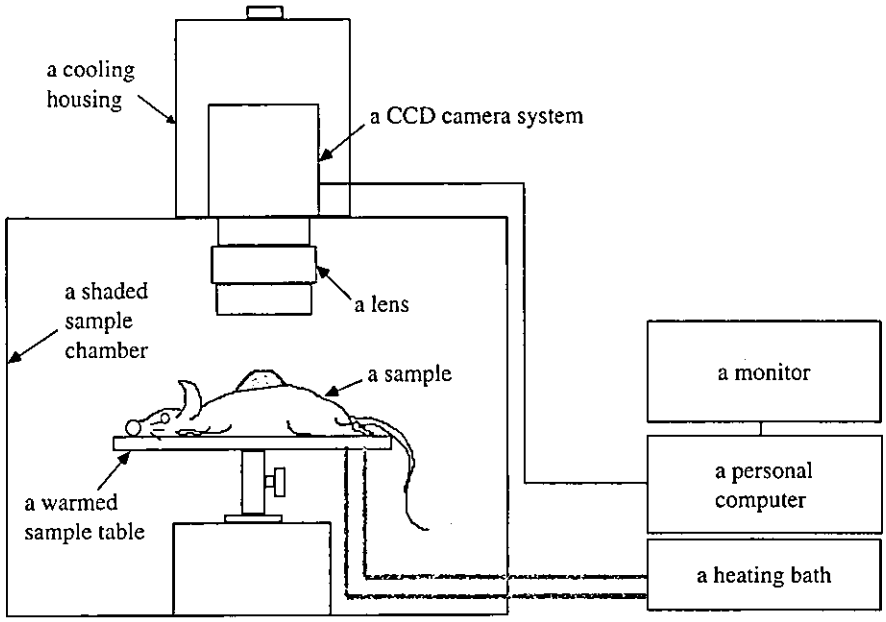

Fig. 1. Schematic of the biophoton imaging system. The biophoton imaging system consists of a liquid nitrogen-cooled highly sensitive CCD camera system (ATC200C, Photometrics), a completely light-shielded sample chamber, a thermostat heater to warm the mice, and a set of computers. The CCD camera system includes a back-illuminated, thinned type Si-CCD (TK1024AB2-G1, Tektronix). The CCD format is 1024×1024 pixels for a full frame, with each pixel size being 24×24 μm. The dark current of the device is 0.225 e⁻/h pixel at −120°C in MPP (multipinned phase) mode and the readout noise is 3.3 e⁻RMS/pixel.

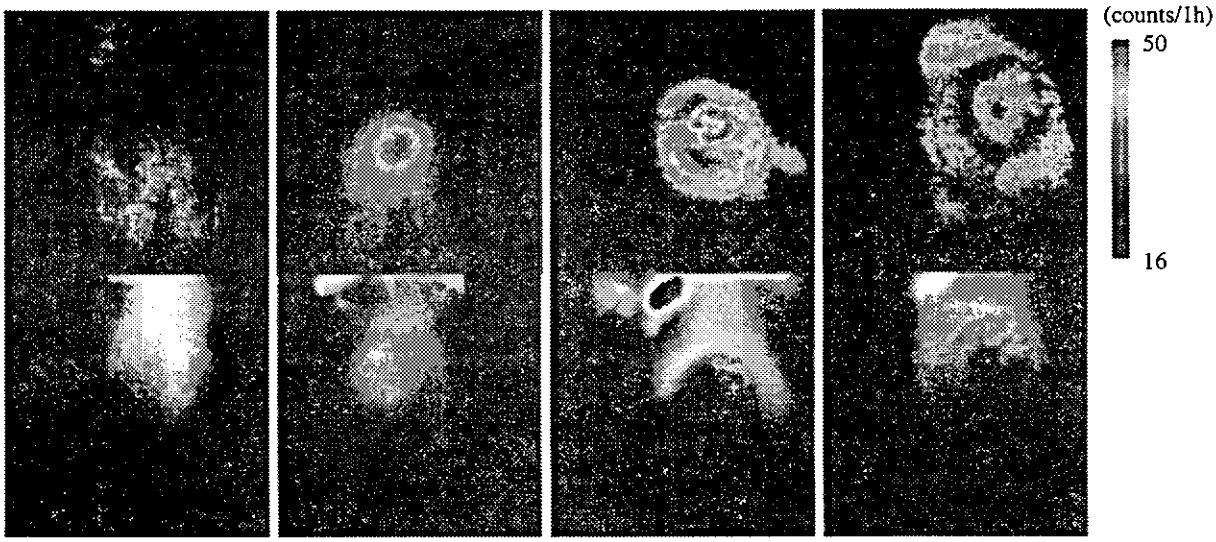

Fig. 2. Biophoton image and pathological findings of AH109A at week 1. The arrows drawn on the tumor corresponds to the cross-sectional line.

the background emission of the mouse determined at a circular region of 600–800 pixels between the blade bones, which exhibited good reproducibility with the lowest biophoton emission in the body of the mice.

Cell lines. The cell lines used in the present study were TE4, TE9 and AH109A. Both TE4 and TE9 are human esophageal carcinoma cell lines established in our department.[13] AH109A is a rat hepatoma cell line.[14] All of the cell lines were cultured in an RPMI1640 medium supplemented with 10% fetal bovine serum. The TE4 and TE9 cells were harvested for transplantation after detachment with trypsin and ethylenediaminetetraacetic acid (EDTA) when the cells were confluent on the bottom of the flasks. The AH109A cells proliferated as a suspension in the medium. The cell suspension was then centrifuged, and cells were collected for transplantation.

Chemicals and animals. We used RPMI1640 medium supplemented with 10% fetal bovine serum (FBS) without phenol red for cell culture. The RPMI1640 medium was purchased from Life Technologies, Inc. (Grand Island, NY) and the FBS was purchased from ICN, Inc. (Costa Mesa, CA). EDTA and trypsin were used to detach the cells from the bottom of the sample cuvettes and culture flasks. The EDTA was purchased from Life Technologies, Inc. and the trypsin was purchased from ICN, Inc. All chemicals were of culture grade.

Mice supplemented in this study were *nu/nu* male nude mice, 5–7 weeks old, purchased from Charles Liver, Inc.

Sample preparation and experimental details. Cells of each line (10^7 cells) were suspended in 0.1 ml of saline (cell volume 0.1

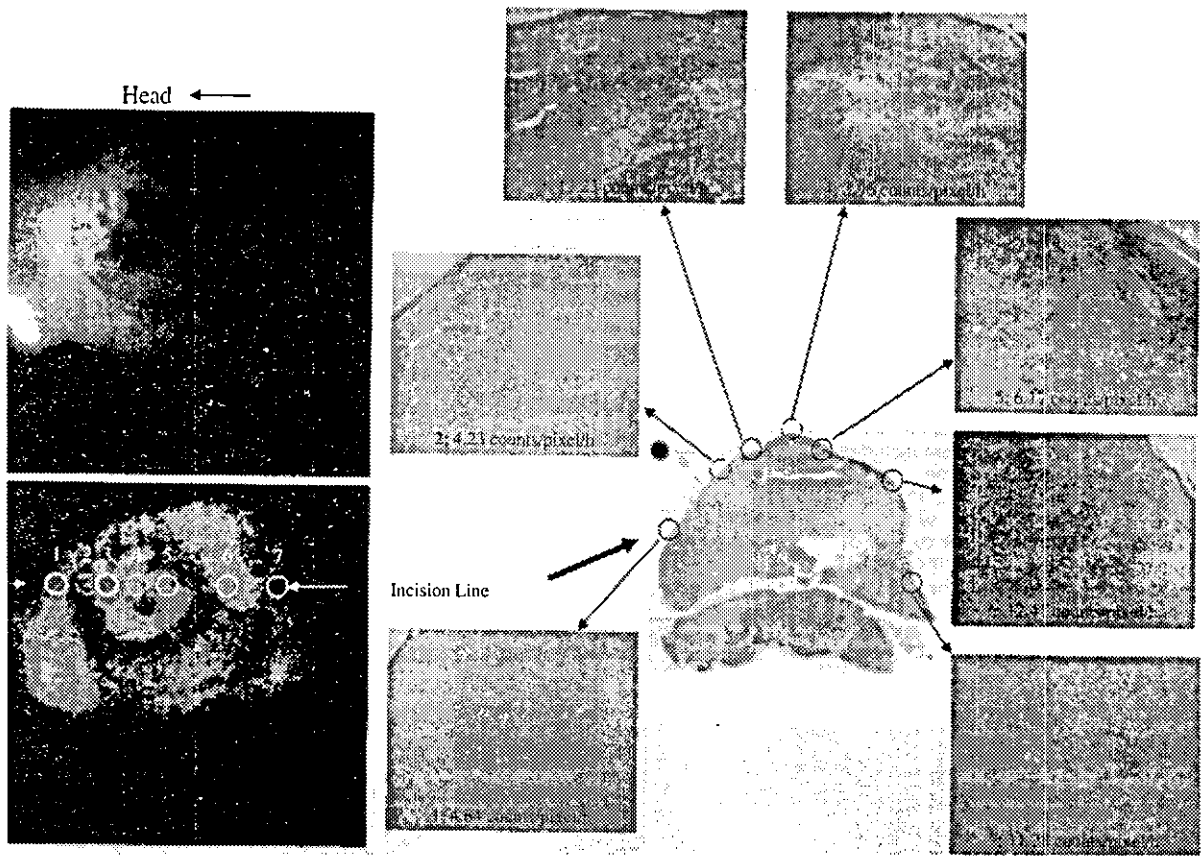

Fig. 3. Changes in the ultraweak biophoton images with tumor growth. Ultraweak biophoton images taken after cell transplantation: week 1, week 2 and week 3.

ml) and 0.2 ml of cell suspension was injected subcutaneously into the backs of the nude mice. After transplantation, the mice were anesthetized with pentobarbital (0.05 mg/g) by intraperitoneal injection and fixed on a temperature-controlled sample table in a completely light-shielded sample chamber. Then biophoton imaging was performed for 1 h with detection of the raw image obtained by a biophoton detector under very weak illumination for estimation of tumor size. Thereafter, the mice were kept in their cages for 1 week and biophoton imaging was performed again for another hour. The correlation between tumor growth rate and biophoton intensity was made at week 1 because AH109A exhibited the fastest growth at that time point; at later times, tumor necrosis appears, and heterogeneity of growth occurs so that the growth rate cannot be properly estimated. Throughout the measurements, the body temperature of the mice was kept at about 37°C.

In some cases the nude mice were kept for 3 weeks for detection of ultraweak biophoton images and pathological examination. After biophoton imaging, the mice were sacrificed by cervical dislocation, and the tumors were excised and embedded in 10% buffered formalin for fixation. We sketched the shape of the tumor mass when we cut the sample for formalin fixation, and we compared the sketch of the pathological sample with the biophoton images. The measurement points of biophoton intensity were carefully identified. Comparison of the biophoton images and pathological slices revealed the relationship between the pathological findings and the two-dimensional biophoton images.

All animal experiments were approved by the Institutional Laboratory Animal Care and Use Committee of Tohoku University. All experiments were performed under UKCCCR guidelines (Workman *et al.*, 1998).[15]

Evaluation of growth rate and statistical analysis. Since the same numbers of cells in the same volume of 0.1 ml were introduced at the point of transplantation, we determined the size of tumors at week 1 to calculate the growth rate. The tumor size at week 1 was estimated from the product of the longest diameter and its perpendicular diameter. Tumor height was not measured at week 1 because the tumor was so thin that it was very difficult to measure.

Estimation of the tumor size and the emission intensity of biophoton images at week 1 were performed for 7 TE9 tumors, 9 TE4 tumors and 17 AH109A tumors. The emission intensity was measured by averaging the total tumor area with subtraction of background biophoton intensity obtained from the data measured at the midpoint of bilateral blade bones on the back of mice (this point exhibited the most stable biophoton intensity in the body throughout the measurement period).

The correlation coefficient was calculated from the biophoton intensity and tumor size (area) or square root of tumor size at week 1.

Biophoton intensity and tumor viability. To compare live and necrotic tumor, we observed 5 AH109A xenografts at 3 weeks. We classified each area into live or necrotic tissue, then we measured the biophoton intensity of corresponding circular areas of 697 pixels in biophoton images (Fig. 3). The intensity was measured in 40 live areas and 26 necrotic areas. Statistical analysis was done with a two tailed *t* test.